GSH-targeted nanosponges increase doxorubicin-induced toxicity "in vitro" and "in vivo" in cancer cells with high antioxidant defenses

GSH-targeted nanosponges increase doxorubicin-induced toxicity ñin vitroò and ñin vivoò in cancer cells with high antioxidant defenses.

Martina Daga[1Ò], Chiara Ulllio[1Ò], Monica Argenziano[2], Chiara Dianzani[2], Roberta Cavalli[2], Francesco Trotta[3], Carlo Ferretti[2], Gian Paolo Zara[2], Casimiro L. Gigliotti[4], Eric S. Ciamporcero[1], Piergiorgio Pettazzoni[1], Denise Corti[5], Stefania Pizzimenti[1*] and Giuseppina Barrera[1].

[1]Department of Clinical and Biological Sciences, University of Turin, Corso Raffaello 30, 10125 Turin (Italy).

[2]Department of Drug Science and Technology, University of Turin, Via P. Giuria 9, 10125 Turin, Italy,

[3]Department of Chemistryï University of Turin, Via Pietro Giuria 7, 10125 Turin, Italy

[4]Department of Health Sciences, University of Eastern Piedmont 'A Avogadro', Via Solaroli 17, 28100 Novara, Italy.

[5]Department of Experimental and Clinical Biomedical Sciences, Biochemistry, Human Health Medical School University of Florence, Viale Morgagni 50, 50134 Florence.

[Ò]M.D. and C.U. contributed equally to this work.

*Corresponding author
Stefania Pizzimenti
Dept. Biological and Clinical Sciences
University of Torino
Corso Raffaello 30
10125 Torino
Tel +39-011-6707763
Fax +39-011-6707763
e-mail: stefania.pizzimenti@unito.it

Abstract

Several reports indicate that chemo-resistant cancer cells become highly adapted to intrinsic oxidative stress by up-regulating their antioxidant systems, which causes an increase of intracellular GSH content. Doxorubicin is one of the most widely used drugs for tumor treatment, able to kill cancer cells through several mechanisms. However, doxorubicin use is limited by its toxicity and cancer resistance. Therefore, new therapeutic strategies able to reduce doses and to overcome chemo-resistance are needed. A new class of glutathione-responsive cyclodextrin nanosponges (GSH-NS), is able to release anticancer drugs preferentially in cells having high GSH content. Doxorubicin-loaded GSH-NS, in the cancer cells with high GSH content, inhibited clonogenic growth, cell viability, topoisomerase II activity and induced DNA damage with higher effectiveness than free drug. Moreover, GSH-NS reduced the development of human tumor in xenograft models more than free drug. These characteristics indicate that GSH-NS can be a suitable drug delivery carrier for future applications in cancer therapy.

Key words

GSH-targeted nanosponges; doxorubicin; prostate and colon cancer cells; toxic effects.

Introduction

Reactive oxygen species (ROS) play an essential role in cellular signaling and several biological and pathological processes, including cancer. The overproduction of ROS in normal cells causes oxidative stress and induces carcinogenesis by amplifying genomic instability [1]; on the contrary, in cancer cells ROS induction can induce cell death.

Compared to normal cells, many types of cancer cells display a large amount of ROS, due to an aberrant metabolism, mitochondrial dysfunction or activation of oncogenes [2]. This characteristic makes cancer cells more vulnerable to damage by further ROS production induced by exogenous agents [2]. In this context, ROS may exert a cytotoxic effect, leading to the death of malignant cells and thus limiting cancer progression [3]. On the basis of these observations, several ROS-generating agents are currently in clinical trials as single agents or in combination therapy [4]. However some cancer cells, in particular those in advanced stages of disease, have become highly adapted to intrinsic oxidative stress by up-regulating their antioxidant systems [5]. This redox adaptation provides a mechanism of resistance to many anticancer agents, due to increased tolerance of exogenous stress and increased capacity for drug inactivation [6]. The extent of antioxidant capacity is actually reported to correlate with the aggressiveness of tumors [7] and it can overcome the antioxidant capacity of normal cells. The major player of oxidative adaptation of cancer cells is the tripeptide glutathione (GSH), which represents the main regulator of the cellular redox status and contributes to drug resistance by binding or reacting to drugs, interacting with ROS, preventing damage to proteins or DNA, or by participating in DNA repair processes [7]. Moreover, GSH is able to modulate cell proliferation, apoptosis, immune function, and fibrogenesis [8]. For these reasons, GSH may constitute a suitable target for the delivery of anticancer drugs specifically to the chemo-resistant cells with high GSH content.

In the past years some GSH-responsive vehicles have been developed to release drugs inside the cells, since the concentration level of GSH in the cytosol is 2 to 3 orders higher (approximately 2ï 10 mM) than the extracellular fluids (approximately 2ï 20 ε M) [9].

Recently it has been suggested that GSH responsive nano-vehicles will eventually be widely applied in targeted cancer therapy, provided that they were composed of biodegradable and/or biocompatible materials [10]. Cyclodextrins (CDs) are biocompatible molecules since they are natural products resulting from intramolecular transglycosylation reactions of starch degraded by cyclodextrin glucanotransferase [11]. They are cyclic Ŭ-1,4-glucans, comprising from six to >100 glucose units, able to form inclusion complexes

and host a wide range of hydrophobic molecules [12, 13]. A novel type of CD nanovehicles are the CD nanosponges (CNs), which are composed of cross-linked cyclodextrin polymers nanostructured in a three-dimensional network. These delivery systems can form complexes with different types of lipophilic or hydrophilic molecules, are safe and biodegradable, display negligible toxicity on cell cultures, and are well-tolerated upon injection in mice [14]. Previous papers reported that CNs are particularly effective in the delivery of some anticancer drugs such as doxorubicin [15] paclitaxel [16] and camptothecin [14]. Cytotoxicity studies showed that camptothecin-loaded in nanosponges was more than 20 times as effective than the free drug in ñin vitroò experiments [14] and reduced, by 70% the growth of prostate cancer cells in mouse xenograft models [17]. It has been suggested that these nanoparticles would accumulate into the tumor site via an Enhanced Permeability and Retention (EPR) effect, which provides sustained release of camptothecin inside the tumor tissue.

Recently, a new class of GSH-responsive CNs (GSH-NS), able to host and to release anticancer drugs in the presence of GSH concentrations similar to those detected in cancer chemo-resistant cells have been developed [18].

In this work we loaded GSH-NS with doxorubicin (Dox-GSH-NS), a well-studied anticancer drug, currently used for a broad spectrum of cancers. However, the employment of doxorubicin (Dox) (or its derivatives) is limited by cardiac and kidney toxicity and by drug resistance, developed by various tumor cells [19]. Thus, the aim of this work was to verify whether the Dox-GSH-NS are able to increase the Dox effect and reduce the effective Dox toxic doses, in particular in the cells characterized by a high GSH content. To pursue this purpose, we looked deeper into the mechanisms of Dox toxicity and compared the anticancer effectiveness of Dox and Dox-GSH-NS in ñin vitroò and ñin vivoò studies.

Material and Methods

Cells, culture conditions and antibodies

HT-29, HCT116, HCT-15 (colon cancer cells), DU145, PC-3 (prostate cancer cells), CAL 62, BHT 101 (thyroid cancer cells), A2058, JR 8 (melanoma cells) and H9c2 rat cardiomyocytes were purchased from American Type Culture Collection (Manassas, VA, USA) and DSMZ (Leibniz-Institut DSMZ, Germany). HT-29, HCT116, HCT15, DU145, PC-3, A2058 and JR8 cells were maintained in a humidified atmosphere of 5% CO2, RPMI-1640 supplemented with 10% FBS and antibiotics, H9c2 and BHT101 cells in DMEM

supplemented with 10% FBS and antibiotics CAL 62 in 50% DMEM plus 50% F12 media supplemented with 10% FBS and antibiotics. The antibodies against Nrf2 and KEAP1 were purchased from Santa Cruz Biotechnology; anti-ß-actin from Sigmaï Aldrich; and anti-HO-1 from Abcam.

Preparation of Dox-GSH-NS

GSH-NS, prepared in-house by prof. Trotta (University of Turin), were obtained by reacting cheap 2-hydroxyethyl disulfide in the presence of ß-cyclodextrin and suitable amount of cross-linking agent (pyromellitic dianhydride). To prepare a nanosponge formulation, 10% w/w coarse-grained aqueous suspension of GSH-NS were homogenized using a piston gap high pressure homogenizer (HPH) (Emulsiflex C5, Avestin, Canada). Subsequently doxorubicin was incorporated by adding to the homogenized nanosponge suspension a doxorubicin hydrochloride solution at the 1:5 (drug:GSH-NS) ratio by weight. The system was incubated at room temperature for 24 h under mild stirring. After 24 h the NS suspension was purified by ultradiafiltration to eliminate the unloaded drug. Tonicity and pH values were corrected to obtain a formulation suitable for the *in vivo* administration.

The nanosponges were characterized by particle size distribution, surface charge, drug loading and in vitro release studies.

Fluorescent-labelled GSH-NS were obtained using the same method but incubating the aqueous nanosuspension with 6-cumarin (ratio 10:0.1 w:w).

Analysis of GSH content

Cells were washed twice with cold 1X PBS, pH 7.4. Total extracts were prepared by lysis in a buffer containing Trisï HCl, pH 7.4, 150 mM NaCl, 5 mM EDTA, 1% TritonX-100, 1 mM PMSF, and 0.05% aprotinin. Insoluble proteins were discarded by high-speed centrifugation at 4°C. Protein concentration in the supernatant was measured in triplicate using a commercially available Bio-Rad protein assay (Bio-Rad Laboratories, SeGSHate, MI, Italy). For the analysis of GSH content, cells (5×10^6) were centrifuged, resuspended in 5% TCA and 5 mM EDTA and the supernatant was added to a 0.4 M Tris-EDTA buffer pH 8.9. The GSH contents were assessed by determining non-protein sulphydryl contents with the Ellmanôs method [20].

ROS detection

ROS detection was performed by a fluorimetric method. Briefly, 10^6 cells were harvested, centrifuged, resuspended in 40 µl of 1X PBS and lysed by sonication. To the cell lysate, 10 µl of 5 εM 2 ', 7' dichlorofluorescein diacetate (DCFH-DA), was added. The mixture was incubated for 20 minutes at 37°C. In this condition, DCFH-DA was hydrolyzed in DCFH not fluorescent, that in the presence of ROS was rapidly oxidized to DCF (2 ', 7'-dichlorofluorescein). The reaction was stopped on ice by adding 1 ml of phosphate buffer (0.1 M, pH 7.4) containing 0.1% Triton X-100. The green fluorescence of DCF was measured by fluorimeter (excitation at 488 nm and emission at 525 nm). The relative concentration of ROS was determined by using a standard curve with scalar amounts of DCF and was expressed as pmol of DCF produced/min/µg of protein.

Analysis of GSH-NS internalization

The GSH-NS internalization was analyzed by using 6-coumarin loaded GSH-NSs. PC-3, DU145, HT-29 and HCT116 cells were cultured in 6-well plates for 24 hours to achieve approximately 80% confluence. Internalization of fluorescent 6-coumarin loaded GSH-NSs, 10 min after addition, was analyzed in a LS510 confocal laser microscope (488 nm exciting laser band 505 to 530 nm bandpass emission filters). Exciting light intensity, black level and photomultiplier were adjusted on control specimen; images were elaborated using LSM510 Image Examiner software (Carl Zeiss).

Cell treatment with Dox or Dox-GSH-NS

Dox (99.9% purity, Sigma) was diluted in the medium at the concentration of 2 mg/ml before each experiment and then further diluted to obtain the final concentration in the well. Cells were treated for 24 hours with increasing concentrations of Dox or Dox-GSH-NS (0.1-2 µg/ml). Thereafter, the medium was removed and cells were resuspended in a complete medium without drug. The treatment with empty GSH-NS was performed to assess the toxicity of vehicle and the values obtained were used as control.

GSH depletion

DU145 cells were exposed to 50 µM Buthionine sulfoximine (BSO) for 24 hours. At the end of this period the GSH concentration was measured as previously described, and the cells were treated with increasing concentration of Dox or Dox-GSH-NS (0.5-2 µg/ml) for 24 hours, then MTT assay was performed.

Analysis of doxorubicin internalization

The internalization of Dox and Dox-GSH-NS was measured at different time points after the drug addition by taking advantage of the red fluorescence of Dox. After incubation for specific times, the cells were collected for measurement of Dox using fluorescence microscopy at 580 nm (Axiovert 35, Zeiss). To quantify the red fluorescence over the time, a cytofluorimetric analysis was performed. Briefly, PC-3 and DU145 cells (2 x 10^5) were treated with 0.5 µM DOX, and HT-29 and HCT116 with 1 µM. Thereafter, the cells were collected, trypsinized and analyzed using a FACScan (Bectonï Dickinson) flow cytometer.

MTT assay

The toxic effect of Dox and Dox-GSH-NS was determined through the 3-(4,5-dimethyl thiazol-2-yl)-2,5-diphenyltetrazolium bromide (MTT) assay. This is a colorimetric assay used to determine the level of metabolic activity in cells able to reduce the yellow tetrazolium dye MTT to purple formazan crystals. The amount of formazan produced an indication of the mitochondrial integrity and activity, which, in turn, may be interpreted as a measure of both cell viability and cell proliferation [21]. MTT analysis was performed in 96-well plates. Cells were seeded (800ï 1500 cells/well) in 200 εl of serum-supplemented medium and treated with Dox or Dox-GSH-NSs for 24 hours. Untreated cells and cells treated with empty GSH-NS were used as control. After this period, the drug was removed and MTT assay was performed. MTT was added to control and treated cells to a final concentration of 0.5 mg/ml (Sigmaï Aldrich) for 2 hours. The medium was then removed, and the cells were lysed with 100 εl of DMSO. Absorbance was recorded at 530 nm by a 96-well-plate ELISA reader.

Colony forming assay

Cells (1000/well) were seeded into a 6-well plate and treated with Dox or Dox-GSH-NS at the concentration of 0.5, 0.2, 0.1, 0.05, 0.02 and 0.01 µg/ml. The medium was changed after 24 hours and cells were cultured for additional 10 days in drug-free medium. Subsequently, cells were fixed and stained with a solution of 80% crystal violet (Sigmaï Aldrich) and 20% methanol. Colonies were photographed and then solubilized in 30% (v/v) acetic acid. Absorbance was recorded at 595 nm by a 96-well-plate ELISA reader.

Cell cycle analysis

Adherent and non-adherent treated and control cells were harvested 24 hours after the treatment with 0.5 µg/ml of Dox or Dox-GSH-NSs. Cells were washed with 1X PBS, fixed in 70% cold ethanol, resuspended in a buffer containing 0.02 mg/ml RNase A (Worthington), 0.05 mg/ml propidium iodide (Sigmaï Aldrich), 0.2% v/v Nonidet P-40 (Sigmaï Aldrich), 0.1% w/v sodium citrate (Sigmaï Aldrich), and analyzed with a FACScan cytometer (Becton Dickinson).

Cell death

Adherent and nonadherent cells were harvested, washed with 1X PBS, and subsequently resuspended in annexin V binding buffer (556454; BD Pharmingen) supplemented with 1:100 APC-conjugated annexin V (550474; BD Pharmingen). Cells were analyzed by a FACSCalibur cytometer (Becton Dickinson).

Western blot assay

Cells were rinsed with ice-cold 1X PBS and lysed on ice in a buffer containing Tris-HCl buffer, pH 7.4, 150mM NaCl, 5mM EDTA, 1% Nonidet P-40, 1mM sodium orthovanadate, 1mM phenylmethylsulfonyl fluoride, and 0.05% aprotinin. Insoluble proteins were discarded by high-speed centrifugation at 4°C. Protein concentration in the supernatant was measured in triplicate using a commercially available assay (Bio-Rad Laboratories, Segrate, Italy). An equal amount of proteins from each lysate was loaded onto SDS-PAGE gels, electrophoresed, and transferred onto PVDF membrane. Following electrotransfer, the membranes were blocked overnight at 4°C in Tris-buffered saline (TBS) containing 5% nonfat dry milk plus 0.5% Tween 20 and then incubated at room temperature with primary antibodies. Visualization of the protein signal was achieved with horseradish peroxidaseï conjugated secondary antibody and enhanced chemiluminescence procedures according to the manufacturerôs protocol (Amersham-Pharmacia Biotech, Italy, Cologno Monzese, Italy). Densitometric analysis was performed by using a software program (Multi-Analyst, version 1.1, Bio-Rad Laboratories, Segrate, Italy). All results were standardized using the signal obtained with ß-actin.

Comet assay

DNA damage was detected by alkaline comet assay, according to a published procedure [22]. The principle behind this assay is that the negatively-charged broken DNA molecules

are free to migrate in an electric field towards the anode, with the shorter fragments moving faster. The pattern of migration produces a profile resembling the shape of a comet. Two main principles determine comet formation patterns: the size of DNA fragments and the number of fragments [23]. To analyze DNA damage, cells were treated, harvested, mixed in agarose gel and plated on a glass slide and incubated at 4°C for 45-60 minutes in lysis solution (2.5 M NaCl, 100 mM Na2EDTA, 10 mM Tris, pH 10.0, Triton X-100 1% v/v, DMSO 10%). The agarose gel slides were washed to neutralize Tris, applied for electrophoresis and DNA was stained with propidium iodide. The distance between the center of the DNA head to the end of the DNA tail, which is called comet tail length and the comet area (total area of the comet subtracted from the nucleus area), as well as the tail area, were used as indicator for DNA damage. These three parameters were calculated with an image analysis software (ImageJ 1.44p, NIH, USA).

Topoisomerase II assay

Commercially available topoisomerase II drug screening kit (TopoGEN, Inc., Columbus, OH) was used. Cells with higher GSH content, namely DU145 and HCT116 cells, were plated at density of about 2 x 10^4 cells / cm^2 and treated the next day with 0.5 µg/ml of Dox or Dox-GSH-NS. After 18 hours, the cells were harvested, washed with 10 mM TRIS-HCl pH 7.5, 1 mM EDTA, 4 mM $MgCl_2$ and 0.5 mM PMSF (TEMP) and resuspended in 1 ml TEMP. Cell nuclei were isolated using a Potter homogenizer type, centrifuged at 1500 rcf for 10 minutes and resuspended in TEMP. The nuclei were washed and resuspended in 10-15 µl of 10 mM TRIS-HCl pH 7.5, 1 mM EDTA, 0.5 mM PMSF (TEP) and an equal volume of 1 M NaCl , then maintained in ice for 45 minutes. At the end, the samples were centrifuged at 18500 RCF for 20 minutes to isolate the supernatant nuclear proteins, including topoisomerase II. Protein quantification was performed by using the commercial kit "Protein assay dye reagent concentrate" (Bio-Rad Laboratories). Each nuclear extract was mixed with 250 ng of "kinetoplast" (kDNA) isolated from Crithidia fasciculata protist, 4 µl of a freshly prepared buffer (0.25 M TRIS-HCl pH 8.0, 0.75 M NaCl, 50 mM $MgCl_2$, 2.5 mM DTT, BSA 150 mg / ml and 10 mM ATP), and H_2O up to a final volume of 15 µl. The mixture was incubated at 37°C for 30 minutes, and the reaction was terminated by the addition of 3 µl of a buffer containing 5% SDS, 0.125% bromophenol blue and 25% glycerol. After incubation, DNA was run on 1% agarose gel containing ethidium bromide (0.5 ug/ml). After electrophoresis, gel was destained in water for 15 min and photographed. Supercoiled DNA, decatenated DNA and linear strand DNA were

incorporated in the gel as markers for DNA topology. The inhibitory activity was calculated as percent of fluorescence reduction of the DNA relaxed bands in treated cells with respect to untreated controls.

In vivo experiments

Du145 cells (10^7) were injected subcutaneously in 6-week-old female Nu+/Nu+ mice (Taconic, Germany). All experimental procedures were done according to Europeans Guidelines and our Institutionôs ethics commission. After 45 days from the injections, when average tumor dimension reached 5 mm^3, mice were randomized in a blind fashion into homogenous groups (5 mice per group) and assigned to different treatments. Dox or Dox-GSH-NS in 10% DMSO solution, were administered by tail injection (200 εl/mouse) at the dose of 5mg/kg, once a week, for 4 weeks. Control mice were injected with empty GSH-NS in 10% DMSO. Treatment related toxicity was determined by monitoring mouse weight weekly.

Euthanasia, collection of tumor samples, and tumor weight determination were performed after 22 days from the beginning of treatments.

Histology and immunohistochemistry

Tumor tissues were fixed in 10% neutral-buffered formalin, paraffin embedded and cut into 5 εm sections. Sections were then deparaffinized, rehydrated and subjected to heat mediated antigen unmasking in 10mM sodium citrate buffer (pH 6.0). Slides were then blocked for one hour with phosphate buffered saline 1% bovine serum albumin, and incubated overnight with the primary antibodies (Ki67 Antibody (SP6), Thermo, MAS 14520). Sections were then incubated in horseradish-conjugated secondary antibodies (Vector Laboratories, Burlingame, CA, USA). Hematoxylin and eosin (Sigma Aldrich, Milan, Italy) staining was performed to assess morphological changes.

Studies of pharmacokinetics and biodistribution

Wistar rats (weighing 250 ± 20 g), were housed under standard conditions with free access to food and water. Dox or Dox-GSH-NS in PBS, were administered by tail injection at the dose of 1 mg/kg. For pharmacokinetics studies, 48 rats were divided randomly into two groups (3 rats per each time point; 8 time points for each treatment) . After treatment, 300 µl blood samples were collected by intrajugular catheter under mild ether anesthesia at the following times: 0, 15 min, 30 min, 45 min, 1 hour, 3 hours and 6 hours. The

samples were then quickly transferred to heparinized tubes, and plasma was immediately separated by centrifugation at 4,000 g for 5 minutes. The plasma samples were stored at ī 20°C for further analysis in HPLC. For the quantitative determination of Dox, 100 ml aliquots of plasma were transferred to clean eppendorf (1.5 ml) tubes, followed by the addition of methanol (100 ml), vortexed for 1 min and sonicated for 5 min. The plasma samples were then centrifuged at 15,000 rpm for 15 min. Subsequently, the supernatants were transferred to new Eppendorf tubes and diluted with 150 ml mobile phase and then centrifuged at 15,000 for 5 min. The supernatants were analyzed by HPLC using a fluorimetric detector (Shimadzu) at a ∂_{exc} = 480nm and ∂_{em} = 560nm with a flow rate of 1ml/min.

To analyze the biodistribution of the two drug formulations, at the desired times after treatments, rats were immediately sacrificed, and their tissues (liver, heart, spleen, lungs, kidney and prostate) were collected, washed with cold saline solution, dried over filter papers, weighed and frozen at - 80°C until analysis. Tissue extracts were prepared by adding one volume of methanol followed by two volumes of Tris buffer 1 M pH 8.5. The mixtures were homogenized and the tissue homogenates allowed to stand in ice for 15 min before adding seven volumes of acetonitrile. The mixtures were vortexed and allowed to stand at room temperature for 15 min before removing the precipitated proteins by centrifugation at 13,000 rpm for 5 min. After centrifugation, clear supernatants (100 µl) were injected after suitable dilution with the mobile phase for HPLC analysis at a ∂_{exc} = 480nm and ∂_{em} = 560nm with a flow rate of 1ml/min. [24].

Statistical analysis

Data were expressed as means ± SD. Significance between experimental groups was determined by one-way ANOVA followed by the Bonferroni multiple comparison post-test using GraphPad InStat software (San Diego, CA, USA). Values of pÒ0.05 were considered statistically significant.

Results

Dox-GSH-NS characterization

Dox-GSH-NS showed an average diameter of 254.7 ± 15.9 nm, a surface charge of - 28. 5 ± 3.0 and a homogeneous size distribution. The pH of the drug- loaded GSH-NS

formulation is 6.0 with a tonicity of about 300 mOSm. Fluorescent-labelled GSH-NS showed the same physico-chemical parameters of doxorubicin-loaded GSH-NS.
The amount of doxorubicin released from the GSH-NS was proportional to the GSH concentration in the receiving phase with increasing release in presence of 10 to 50 mM GSH as previously shown [18].

Analysis of basal level of GSH, ROS and antioxidant proteins

To establish the oxidative stress level, we analyzed the GSH concentration (Fig 1A) in several human cancer cell lines from diverse types of cancers (colon, prostate, thyroid, melanoma). Among the different lines, DU145 and HCT116, prostate and colon cancer cells, which displayed the highest GSH content, and PC-3 and HT-29, cancer cells of similar origin, with a low GSH content, were selected for the further experiments. In the latter, the basal level of ROS was detected by fluorimetric analysis of the DCF fluorescent production (Fig. 1B). Results obtained demonstrated that the ROS level was inversely related to GSH content. Indeed, PC-3 and HT-29 cells, which displayed a low level of GSH content, had a higher level of ROS than DU145 and HCT116 cells.
This observation suggested that the antioxidant potential of DU145 and HCT116 cells was higher than that of PC-3 and HT-29. Since the master regulator of antioxidant enzymes, also involved in GSH synthesis, is nuclear factor erythroid 2ï related factor 2 (Nrf2) transcription factor, together with its inhibitor, Kelch-like erythroid cell-derived protein with CNC homology-associated protein 1 (Keap-1), we investigated, in these cell lines, the expression of Nrf2, Keap-1 and the expression of heme oxigenasi-1 (HO-1) protein, whose gene is a target of Nrf2 transcription factor (Fig. 1, Supplementary data). Results demonstrated that in DU145 and HCT116 cells the basal expression of Nrf2, was higher than that detected in PC-3 and HT-29. On the contrary, the level of Keap1 was lower in DU145 and HCT116 cells than in PC-3 and HT-29 cells. According to the amount of Nrf2 protein, the expression of the Nrf2 target, HO-1, is higher in DU145 and HCT116 cells with respect to PC-3 and HT-29 cells. These data confirm that DU145 and HCT116 have a higher antioxidant potential, in accordance with the higher level of GSH found in these two lines.

Analysis of the GSH-NS and DOX-GSH-NS internalization

To detect the internalization of GSH-NSs into the cells, we performed a confocal microscopy analysis by using 6-coumarin-loaded GSH-NSs. The fluorescent nanoparticles

were internalized within 10 minutes into all types of cells, with a slight difference for some PC-3 cells in which the fluorescence was evident, at this time point, mainly at the plasma membrane level (Fig 2 A). The time course of Dox and Dox-GSH-NS incorporation was performed by visualization of red fluorescence by using a fluorescence microscope. Results indicated that free Dox was internalized more slowly than the drug carried by GSH-NS in all types of cells examined (Fig. 2 B). Indeed, the red fluorescence was evident starting from 15 minutes with Dox-GSH-NS, whereas only a slight red fluorescence was evident after 120 minutes in cells treated with the free drug, except HCT116 in which fluorescence was evident only after 4 hours (data not shown).

The fluorescence intensity was measured by cytofluorimetric analysis also. Data, expressed as percent of red fluorescence in control cells, are in agreement with the observations by the fluorescence microscopy, indicating that the Dox internalization by all of the cell lines is faster when carried by GSH-NS (Fig.2, Supplementary data).

Effect of Dox and Dox.GSH-NS on cell proliferation and cell cycle distribution

To test the response of cells to the two doxorubicin formulations, we first analyzed cell viability after an exposure of 24 hours to high concentrations (2, 1, 0.5 µg/ml) of Dox or Dox-GSH-NS. MTT analysis revealed that cells with higher concentrations of GSH, namely DU145 and HCT-116 cells, were more affected by Dox-GSH-NS than the drug in free form at all concentrations used (Fig.3). To the contrary, PC-3 and HT-29 cells did not show a different response to the treatment with the two doxorubicin formulations. The empty GSH-NS did not show any toxicity even at highest doses, and the MTT values were similar to those obtained in untreated cells (data not shown).

To assess whether the lowering of the GSH concentration could affect the toxic effect of Dox or Dox-GSH-NS, DU145 cells, were exposed to 50 µM BSO for 24 hours, then the GSH concentration was measured (Fig.4A). The treatment with BSO reduced by about 70% the GSH cell content. BSO-exposed cells were then treated with increasing concentrations of DOX or Dox-GSH-NS and, after the subsequent 24 hours, an MTT assay was performed (Fig. 4B). In BSO-exposed cells, an increase of the Dox toxic effect and a slight reduction of the Dox-GSH-NS effect, at the highest drug concentration, were observed. These modifications reduced the differences in toxicity between the two drug formulations, thus annulling the higher effectiveness of Dox-GSH-NS in DU145 cells.

The clonogenic assay tested the effectiveness of low doxorubicin concentrations (0.5, 0.2, 0.1, 0.05, 0.02 µg/ml) in cells exposed for 24 hours to the drug in free form or carried by GSH-NSs (Fig.5).

Both Dox and Dox-GSH-NS inhibited colony formation almost completely at the concentrations of 0.5, 0.2 and 0.1 µg/ml. Interestingly, Dox-GSH-NS was more effective than Dox at the lowest concentrations (0.05 and 0.02 µg/m) in DU145 and HCT116 cells.

To investigate whether the different degree of the inhibition of proliferation depended on the inhibition of cell cycle progression, the cell cycle analysis was performed 24 hours after the treatment with Dox or Dox-GSH-NS (0.5 µg/ml). Dox induced, in all cell lines, a reduction of G0/G1 cells and an increase of cells in the G2/M phase of the cell cycle (Fig.6). However, while in PC-3 and HT-29 cells, the amount of G2/M cells was similar after the treatment with both doxorubicin formulations, in DU145 and HCT116 cells, the amount of G2/M cells was higher after treatment with Dox-GSH-NS than Dox.

Cell death and DNA damage

A number of models have been proposed for doxorubicin-mediated cell death, including oxidative stress induction, DNA adduct formation, and topoisomerase II poisoning [25]. To determine the amount of the cell death induced by high concentrations of Dox, in both formulations, annexin V-positive cells were analyzed 24 hours after the treatment with the drug at the concentration of 2 µg/ml (Fig. 7).

While, the amount of annexin positive cells was similar in PC-3 and HT-29 cells after treatment with Dox or Dox-GSH-NS, in DU145 and HCT116 cells, the amount of annexin V-positive cells, after treatment with doxorubicin loaded-GSH-NSs was higher than that obtained after treatment with free doxorubicin.

To verify whether the increase of cell death in DU145 and HCT116 cells was related to the increase of oxidative stress induced by Dox-GSH-NS with respect to Dox, the ROS production was measured in these cell lines 24 hours after treatment with 1 µg/ml of Dox or Dox-GSH-NS (Fig.8). The ROS content was significantly increased in both cell lines after Dox-GSH-NS treatment, compared with Dox, suggesting that the increased cell death in these cell lines could be related to the increase of oxidative stress.

The induction of DNA damage in Dox-treated cells has been extensively demonstrated. The topoisomerase II-mediated DNA strand breaks play a key role in the doxorubicin-induced cytotoxicity [26]. Topoisomerases catalyze DNA unwinding for transcription and replication, which involves formation of an intermediate called the ñcleavable complex.ò

Dox binds the topoisomerase II cleavable complex, resulting in double-strand DNA breaks [27]. The effects of Dox and Dox-GSH-NS (0.5 µg/ml) on topoisomerase II activity was determined in DU145 and HCT116, 18 hours after the treatment. Nuclear extracts were added to KDNA (kinetoplast DNA) and the amount of DNA decatenation was examined. Results obtained demonstrated that the decatenation of DNA (indicated by arrows) was more inhibited in both cell lines when treated with Dox-GSH-NSs (by 85 and 79% in HCT116 and DU145 cells, respectively) than after treatment with free Dox (Fig.9).

To assess the amount of DNA damage after Dox and Dox-GSH-NS treatments we performed the single cell electrophoresis assay (comet assay) which has been extensively used to detect DNA damage induced by hyperthermia and radiation [28] and DNA repair, supercoiling and replication [29].

Comet assay was performed 24 hours after treatment with 1 µg/ml of Dox or Dox-GSH-NS (Fig. 9). While comets originating from the controls have a nearly symmetrical shape and practically no tails, comets from cells treated with doxorubicin are characterized by fairly long tails. This difference was especially prominent in DU145 and HCT116 cells after Dox-GSH-NS treatment (Fig. 10, panels A and C). By using image analysis software, we have calculated the comet tail length (the distance between the center of the DNA head to the end of the DNA tail), the comet area (total area of the comet subtracted from the nucleus area), as well as the tail area. These three parameters were used as an indicator of DNA damage. Results confirmed the higher effect, displayed by Dox-GSH-NS, with respect to Dox, in DU145 and HCT116 cells (Fig. 10, panel B and D).

Biodistribution, pharmacokinetics and toxicity of Dox-GSH-NS on rat cardiomyocytes.

The plasma concentrationï time profiles following single dose i.v. administration of Dox and Dox-GSH-NS was analyzed. Dox was rapidly cleared from the circulation within 30 min, whereas Dox-GSH-NS was still present. Dox-GSH-NS exhibited a prolonged plasma circulation time, showing a detectable plasma concentration after 6 hours from the administration (Fig. 11 C).

Biodistribution of Dox and Dox-GSH-NS in rat organs was determined at 0.5, 3 and 6 hours after i.v. administration (Fig.11 A, B). Dox and Dox-GSH-NS accumulated in the liver, spleen, kidney and heart with a low amount in the lung and prostate. However, a lesser distribution in the heart was observed from Dox-GSH-NS compared to Dox, in particular, at 3 hours after the treatment. At this time point the Dox-GSH-NS concentration in heart was significantly lower than that detected after Dox treatment.

Dox and Dox-GSH-NS anticancer effect in xenograft tumor model.

To assess the anticancer effect of Dox and Dox-GSH-NS in ñin vivoò experiments, we implanted DU145 cells, the cell line with the highest biological response to Dox-GSH-NS, in Nu+/Nu+ mice and we treated animals with the two drug formulations. Results obtained demonstrated that tumor weights were significantly reduced by Dox-GSH-NS treatment with respect to Dox which, in turn, slightly reduced tumor weight with respect to the controls. Interestingly, Ki67 staining indicated that the reduction of proliferative cells is even more marked than the reduction of tumor weight. Indeed, the percentage of Ki67 positive cells, counted in 1 mm^2 of stained slide was 46.17% in control, 22.18% in Dox treated tumors and 9.0% in Dox-GSH-NS treated tumors.

The ematoxilin-eosin stained slides showed, in the control, a compact mass of tumor cells interspersed with thin trabeculae of connective tissue; in Dox treated tumors, beside tumor cells, some necrotic areas were present; in GSH-NS-Dox treated tumors the necrotic areas were increased and the tumor cells were reduced and replaced by fibroblasts.

DISCUSSION

Various polymeric vehicles, developed in the past years as carriers for antitumor drugs, such as Dox or paclitaxel, demonstrated inadequate stability [30, 31] or inadequate toxicity against tumor cells compared with the drug alone [32]. Dox-GSH-NS, on the contrary, increased Dox toxicity in cells with high GSH content and did not reduce Dox toxicity in the other cancer cells. Moreover, this type of nanosponge comprises carbonate bonds and disulfide bridges which can be open in a reducing environment. However, when the high GSH concentration provokes the opening of the disulfide bridges and promotes the outflow of the drug, the structure of GSH-NS is almost maintained by the carbonate bonds.

We have demonstrated that these GSH-NS can be easily uptaken by the cells and penetrate more quickly than free Dox, as demonstrated by microscopy and cytofluorimetric analysis of Dox red fluorescence. The rapid internalization of GSH-NS did not depend on the type of cells treated, because, with slight differences, Dox-GSH-NS were completely internalized in all cell lines within 2 hours. Our results demonstrated that GSH-NS can be internalized, as other cyclodextrin nanosponges, but they take advantage of disulfide bridges, which increase the release the drug in the presence of high antioxidant concentration [18]. As a consequence , Dox-GSH-NS, by releasing the drug more easily in the cells with high antioxidant potential, targets the cells which posses a higher ability of Dox detoxification, adding a significant specificity to the drug action.

The Dox internalization is essential for the drug to be effective in tumor therapy. After internalization, Dox-GSH-NS was also able to increase Dox effectiveness at low doses, as demonstrated in colony forming assay, after cell exposure for a limited time (24 hours) to the low concentrations of free Dox or Dox-GSH-NS (0.05 and 0.02 µg/ml). At these low concentrations, Dox-GSH-NS significantly reduced colony formation in DU145 and HCT116 cells compared to Dox , until 10 days after the addition.

Dox-GSH-NS in addition to maintaining the drug toxicity over the time period, determined a fast action of drug in the cells with high GSH content, as demonstrated by experiments performed 24 hours after the treatment with high drug doses. In these experiments, Dox-GSH-NS displayed a greater effect than Dox in DU145 and HCT116 cells, by reducing cell viability, and by inducing G2/M cell accumulation and cell death. Moreover, the increase in the DNA damage, demonstrated by comet assay, also confirms that Dox-GSH-NS was more effective than Dox in cells with high GSH content. In these cells, both the increase of cell death and the G2/M accumulation can be due to the formation of DNA adducts [33] and topoisomerase II poisoning [34]. Interestingly, when the GSH content was reduced by BSO treatment, the Dox-GSH-NS toxic effect became similar to that determined by the free drug.

It has been demonstrated for several types of nanoparticles that they are unable to penetrate through endothelial junctions of normal blood vessels, thus increasing their concentration in the plasma and rendering them a long plasma half-life [35].

The pharmacokinetic results confirmed these observations, demonstrating that Dox-GSH-NSs exhibited a prolonged plasma circulation time compared to free Dox. Moreover, drug-loaded nanoparticles can selectively extravasate in tumor tissue, due to their abnormal vascular nature. The selective accumulation of drug loaded nanoparticles in tumor tissue has long been known as the enhanced permeability and retention (EPR) effect [36]. From this point of view, the increase plasma circulation of Dox-GSH-NS might further enhance drug accumulation in tumor tissue.

The high effectiveness of Dox-GSH-NS with respect to Dox has been confirmed by the ñin vivoò experiments, performed in mice transplanted with DU145 cells. Not only, was Dox-GSH-NS more effective than Dox in reducing tumor growth, in terms of tumor weight, but also, Dox-GSH-NS highly reduced the number of proliferating Ki67 positive-cells, which were about 9% of total cells in Dox-GSH-NS-treated mice, whereas this percentage increased to 22% in Dox-treated mice and 46% in control mice.

The major adverse effect of doxorubicin administration is the cardiotoxicity, which may limit its use. In mice transplanted with DU145 cells we did not observe signs of acute doxorubicin cardiotoxicity which can occur during and within 2ï 3 days of its administration [37]. Moreover, the biodistribution of Dox-GSH-NS demonstrated that heart accumulation of Dox-GSH-NS was significantly lower than that observed in Dox-treated animals; and the experiments performed on rat cardiomyocytes, by using the same dose of Dox and Dox-GSH-NS, showed that the toxicity of these two formulations was similar.

In conclusion, GSH-NSs, which are rapidly internalized by cancer cells of different origins, increased the chemotherapeutic effect of Dox in cells having high antioxidant content, both in ñn vitroòand ñn vivoòexperiments, without evidence of a significant organ toxicity.

Since the increase of antioxidant potential is one of the main mechanisms of resistance toward many anticancer agents [6], this delivery system seems to be particularly useful in targeting chemo-resistant tumors. Moreover, the fact that Dox-GSH-NS can affect cell proliferation at doses lower than Dox in free form, allows a reduction of effective drug doses and, of consequence, of the systemic adverse effects. All these characteristics suggest that GSH-NSs can be a suitable drug delivery carrier for future applications in cancer therapy.

Acknowledgements

This work was supported by the University of Turin (ex 60% by Barrera, Cavalli, Dianzani) and by Progetti di Ricerca di Ateneo ï Anno 2011. We thank Dr. Angelo Cerbone for his helpful advice on Comet assay.

References

[1]. Wang, J.; Yi, J. Cancer cell killing via ROS: to increase or decrease, that is the question. Cancer. Biol. Ther. 7:1875-1884; 2008.

[2]. Pelicano, H.; Carney, D.; Huang, P. ROS stress in cancer cells and therapeutic implications. Drug Resist. Updat. 7:97-110; 2004.

[3]. Fruehauf, J. P.; Meyskens, F. L., Jr. Reactive oxygen species: a breath of life or death? Clin. Cancer Res. 13:789-794; 2007.

[4]. Cabello, C. M.; Bair, W. B., 3rd; Wondrak, G. T. Experimental therapeutics: targeting the redox Achilles heel of cancer. Curr. Opin. Investig. Drugs 8:1022-1037; 2007.

[5]. Barrera, G. Oxidative stress and lipid peroxidation products in cancer progression and therapy. ISRN Oncol. 2012:137289; 2012.

[6]. Trachootham, D.; Alexandre, J.; Huang, P. Targeting cancer cells by ROS-mediated mechanisms: a radical therapeutic approach? Nat. Rev. Drug Discov. 8:579-591; 2009.

[7]. Traverso, N.; Ricciarelli, R.; Nitti, M.; Marengo, B.; Furfaro, A. L.; Pronzato, M. A.; Marinari, U. M.; Domenicotti, C. Role of glutathione in cancer progression and chemoresistance. Oxid. Med. Cell. Longev. 2013:972913; 2013.

[8]. Lu, S.C. Glutathione synthesis. Biochim. Biophys. Acta 1830:3143-53; 2013.

[9]. Schafer, F. Q.; Buettner, G. R. Redox environment of the cell as viewed through the redox state of the glutathione disulfide/glutathione couple. Free Radic. Biol. Med. 30:1191-1212; 2001.

[10]. Cheng, R.; Feng, F.; Meng, F.; Deng, C.; Feijen, J.; Zhong, Z. Glutathione-responsive nano-vehicles as a promising platform for targeted intracellular drug and gene delivery. J. Control. Release 152:2-12; 2011.

[11]. Takada, M.; Nakagawa, Y.; Yamamoto, M. Biochemical and genetic analyses of a novel gamma-cyclodextrin glucanotransferase from an alkalophilic Bacillus clarkii 7364. J. Biochem. 133:317-324; 2003.

[12]. Szejtli, J. Introduction and General Overview of Cyclodextrin Chemistry. Chem. Rev. 98:1743-1754; 1998.

[13]. Trotta, F.; Zanetti, M.; Cavalli, R. Cyclodextrin-based nanosponges as drug carriers. Beilstein J. Org. Chem. 8:2091-2099, 2012.

[14]. Minelli, R.; Cavalli, R.; Ellis, L.; Pettazzoni, P.; Trotta, F.; Ciamporcero, E.; Barrera, G.; Fantozzi, R.; Dianzani, C.; Pili, R. Nanosponge-encapsulated camptothecin exerts anti-tumor activity in human prostate cancer cells. Eur. J. Pharm. Sci. 47:686-694; 2012.

[15]. Cavalli, R.; Trotta, F.; Tumiatti, W. Cyclodextrin-based nanosponges for drug delivery. J. Inclusion Phenom. 56:209-213; 2006.

[16]. Namgung, R.; Mi Lee, Y.; Kim, J.; Jang, Y.; Lee, B. H.; Kim, I. S.; Sokkar, P.; Rhee, Y. M.; Hoffman, A. S.; Kim, W. J. Poly-cyclodextrin and poly-paclitaxel nano-assembly for anticancer therapy. Nat. Commun. 5:3702, 2014. doi: 10.1038/ncomms4702.

[17]. Gigliotti, C.L.; Minelli, R.; Cavalli, R.; Occhipinti, S.; Barrera, G.; Pizzimenti, S.; Cappellano, G.; Boggio, E.; Conti, L.; Fantozzi, R.; Giovarelli, M.; Trotta, F.; Dianzani, U.; Dianzani, C. In vitro and in vivo therapeutic evaluation of camptothecin-encapsulated ɓ-cyclodextrin nanosponges in prostate cancer. J Biomed. Nanotech., 12: 114-127, 2016.

[18]. Trotta, F.; Caldera, F.; Dianzani, C.; Argenziano, M.; Barrera, G.; Cavalli, R. New Glutathione Bio-Responsive Cyclodextrin Nanosponges. ChemPlusChem cplu.201500531. DOI: 10.1002/cplu.201500531

[19]. Minotti, G.; Menna, P.; Salvatorelli, E.; Cairo, G.; Gianni, L. Anthracyclines: molecular advances and pharmacologic developments in antitumor activity and cardiotoxicity. Pharmacol. Rev. 56:185-229; 2004.

[20]. Ellman, G. L. Tissue sulfhydryl groups. Arch. Biochem. Biophys. 82:70-77; 1959.

[21]. Sylvester, P. W. Optimization of the tetrazolium dye (MTT) colorimetric assay for cellular growth and viability. Methods Mol. Biol. 716:157-168; 2011.

[22]. Zhou, B. B.; Elledge, S. J. The DNA damage response: putting checkpoints in perspective. Nature 408:433-439; 2000.

[23]. Husseini, G. A.; O'Neill, K. L.; Pitt, W. G. The comet assay to determine the mode of cell death for the ultrasonic delivery of doxorubicin to human leukemia (HL-60 cells) from Pluronic P105 micelles. Technol. Cancer Res. Treat. 4:707-711; 2005.

[24]. Fundarò, A.; Cavalli, R.; Bargoni, A.; Vighetto, D.; Zara, G.P., Gasco, M.R. Non-stealth and stealth solid lipid nanoparticles (SLN) carrying doxorubicin: pharmacokinetics and tissue distribution after i.v. administration to rats. Pharmacol Res. 42:337-343, 2000.

[25]. Yang, F.; Teves, S. S.; Kemp, C. J.; Henikoff, S. Doxorubicin, DNA torsion, and chromatin dynamics. Biochim. Biophys. Acta 1845:84-89; 2013.

[26]. Kalet, B. T.; McBryde, M. B.; Espinosa, J. M.; Koch, T. H. Doxazolidine induction of apoptosis by a topoisomerase II independent mechanism. J. Med. Chem. 50:4493-4500; 2007.

[27]. Liu, L. F.; Rowe, T. C.; Yang, L.; Tewey, K. M.; Chen, G. L. Cleavage of DNA by mammalian DNA topoisomerase II. J. Biol. Chem. 258:15365-15370; 1983.

[28]. Fairbairn, D. W.; Olive, P. L.; O'Neill, K. L. The comet assay: a comprehensive review. Mutat. Res. 339:37-59; 1995.

[29]. Vogelstein, B.; Pardoll, D. M.; Coffey, D. S. Supercoiled loops and eucaryotic DNA replicaton. Cell 22:79-85; 1980.

[30]. Toncheva, V.; Schacht, E.; Ng, S. Y.; Barr, J.; Heller, J. Use of block copolymers of poly(ortho esters) and poly (ethylene glycol) micellar carriers as potential tumour targeting systems. J. Drug Target. 11:345-353; 2003.

[31]. Liu, J.; Zeng, F.; Allen, C. Influence of serum protein on polycarbonate-based copolymer micelles as a delivery system for a hydrophobic anti-cancer agent. J. Control. Release 103:481-497; 2005.

[32]. Matsumura, Y.; Hamaguchi, T.; Ura, T.; Muro, K.; Yamada, Y.; Shimada, Y.; Shirao, K.; Okusaka, T.; Ueno, H.; Ikeda, M.; Watanabe, N. Phase I clinical trial and pharmacokinetic evaluation of NK911, a micelle-encapsulated doxorubicin. Br. J. Cancer 91:1775-1781; 2004.

[33]. Swift, L. P.; Rephaeli, A.; Nudelman, A.; Phillips, D. R.; Cutts, S. M. Doxorubicin-DNA adducts induce a non-topoisomerase II-mediated form of cell death. Cancer Res. 66:4863-4871; 2006.

[34]. Larsen, A. K.; Escargueil, A. E.; Skladanowski, A. From DNA damage to G2 arrest: the many roles of topoisomerase II. Prog. Cell Cycle Res. 5:295-300; 2003.

[35]. Greish, K. Enhanced permeability and retention (EPR) effect for anticancer nanomedicine drug targeting. Methods Mol Biol. 624:25-37, 2010.

[36]. Maeda, H.; Nakamura, H.; Fang, J. The EPR effect for macromolecular drug delivery to solid tumors: Improvement of tumor uptake, lowering of systemic toxicity, and distinct tumor imaging in vivo. Adv Drug Deliv Rev. 65:71-9, 2013.

[37]. Takemura, G.; Fujiwara, H. Doxorubicin-induced cardiomyopathy from the cardiotoxic mechanisms to management. Prog Cardiovasc Dis. 49:330ï 352, 2007.

FIGURE LEGENDES

Fig. 1. Panel A**:** Analysis of GSH content in untreated cancer cells. GSH levels are expressed as μg of GSH per mg of protein. Values are the mean ± SD of 3 separate evaluations. Panel B: ROS content analysis in untreated cells. DCFH-DA was added to cell lysates and DCF, produced by DCFH oxidation by ROS, was measured by fluorimeter (excitation at 488 nm and emission at 525 nm). The relative concentration of ROS was determined by using a standard curve with scalar amounts of DCF and was expressed as pmol of DCF produced/min/μg of protein. Values are the mean ± SD of 3 separate evaluations. §§§ p value Ò0.001 vs. PC-3 cells. *** p value Ò0.001 vs. HT-29 cells.

Fig. 2. Panel A: Cell uptake of fluorescent coumarinated GSH-NS in DU145, PC-3, HCT116 and HT-29 cells. Cells were incubated with GSH-NS for 10 minutes and then analyzed by confocal laser scanning microscopy without fixation.
Panel B: Internalization of Dox and Dox-GSH-NS. DU145, PC-3, HCT116 and HT-29 cells were collected after 15 and 120 min from the treatment with 0.5 μg/ml of Dox or Dox-GSH-NS. Red fluorescence of doxorubicin was examined by using a fluorescence microscopy (580 nm).

Fig.3. Dox and Dox-GSH-NS toxicity evaluated by MTT assay in DU145, PC-3, HCT116 and HT-29 cells. Results are expressed as percent of inhibition of control values, obtained after 24 hours of treatment with 2, 1, 0.5 μg/ml of Dox or Dox-GSH-NS and are the mean ± SD of four separate experiments. Untreated cells and cells treated with empty GSH-NS were used as controls for the cells treated with Dox or Dox-GSH-NSs, respectively.
***pÒ0.001vs Dox.

Fig 4 Panel A**:** Analysis of GSH content in untreated DU145 cells (C) and treated with 50 μM BSO (BSO) for 24h. GSH levels are expressed as μg of GSH per mg of protein. Values are the mean ± SD of 3 separate evaluations. **pÒ0.01 vs C.
Panel B: Table 1. Dox and Dox-GSH-NS toxicity evaluated by MTT assay in DU145 cells, expressed as percent of inhibition with respect to the control values, obtained 24 hours after treatment with 2, 1, 0.5 μg/ml of Dox or Dox-GSH-NS in cells exposed to 50 μM BSO (with BSO) or in controls (w/o BSO). Values are the mean ± SD of 3 separate experiments.***pÒ0.001vs Dox.

Fig. 5 Clonogenic assay. DU145, PC-3, HCT116 and HT-29 cells were treated with 0.5, 0.2, 0.1, 0.05 and 0.02 μg/ml of Dox or Dox-GSH-NS. Cells were exposed for 24 hours to the drug, washed and then cultured for an additional 10 days in doxorubicin free medium. Panel A: Colony forming images of DU145, PC-3, HCT116 and HT-29 cells 10 days after exposure to Dox or Dox-GSH-NS at concentrations of 0.02, 0.05, 0.1 μg/ml. Panel B. After acquisition of images, colonies were solubilized and cell density were quantified by absorbance at 595 nm. Values obtained are expressed as percent of inhibition of absorbance values with respect to the relative control values (untreated cells and cells treated with empty GSH-NS) and are the mean ± SD of four separate experiments. **pÒ0.01 vs Dox.

Fig.6. Percent of cell in cell cycle phases 24 hours after treatment with 0.5 µg/ml of Dox or Dox-GSH-NS. C: control; GSH-NS: empty GSH-nanosponges. Data are the mean ± SD of 3 separate experiments.
***pÒ0.001, **pÒ0.01, *pÒ0.05 vs Dox.

Fig.7. Cell death. DU145, PC-3, HCT116 and HT-29 cells were treated with 2 µg/ml of Dox, Dox-GSH-NS or untreated (C). Data are the mean ± SD of 3 separate experiments. ***pÒ0.001vs C.

Fig 8. ROS production in DU145 and HCT116 cells and in untreated cells (C). Cells were treated with 1 µg/ml Dox or Dox-GSH-NS. Data are the mean ± SD of 3 separate experiments, expressed in arbitrary units, where control values were set at 1. **pÒ0.01 vs Dox.

Fig.9. Topoisomerase II analysis in HCT116 and DU145 cells 18 hours from the treatment with 0.5 µg/ml of Dox or Dox-GSH-NS. Lane 1, KDNA without topoisomerase II (catenated form); lane 2, KDNA with topoisomerase II (decatenated form), Lane 3: linear DNA; line 4: control; lane 5: Cells treated with Dox; lane 6: cells treated with Dox-GSH-NS.

Fig.10. Comet assay. DU145, PC-3, HCT116 and HT-29 cells were treated with 1 µg/ml of Dox or Dox-GSH-NS or untreated (C). Panel A and C: Representative comet assays in the indicated cell lines; Panel B and D: comet tail length, comet area and tail area, calculated with an image analysis software, are expressed in arbitrary units, where control values were set at 1.
*** p Ò0.001 vs. C; *pÒ0.05 vs. C; §§§ pÒ0.001 vs. Dox; § pÒ0.05 vs. Dox

Fig 11. Panel A and B Tissue distribution of doxorubicin after i.v. administration to rats of 1 mg/kg of Dox or Dox-GSH-NS. ***pÒ0.001vs Dox
Panel C. Plasma concentration of doxorubicin after i.v. administration to rats of 1 mg/kg of Dox or Dox-GSH-NS. Panel D: Dox and Dox-GSH-NS toxicity evaluated by MTT assay in H9c2 cells, 24 hours after treatment with 2, 1, and 0.5 µg/ml of Dox or Dox-GSH-NS. Results are expressed as percent of inhibition of control values and are the mean ± SD of 3 separate experiments.

Fig. 12. Panel A: weight of tumor 20 days after subcutaneous transplantation of 10^7 DU145 cells in N+/N+ mice. Treatment with Dox or Dox-GSH-NS 5 mg/kg (10% DMSO + H_20) started from 45 days after the transplant (tumor mass ~ 5 mm) and was performed once a week, for 4 weeks, through tail injection (200 εl/mouse). ** p<0.01 Dox-GSH-NS vs Dox. Panel B: IHC and H&E on paraffin embedded tumors.

Figure 1

Click here to download high resolution image

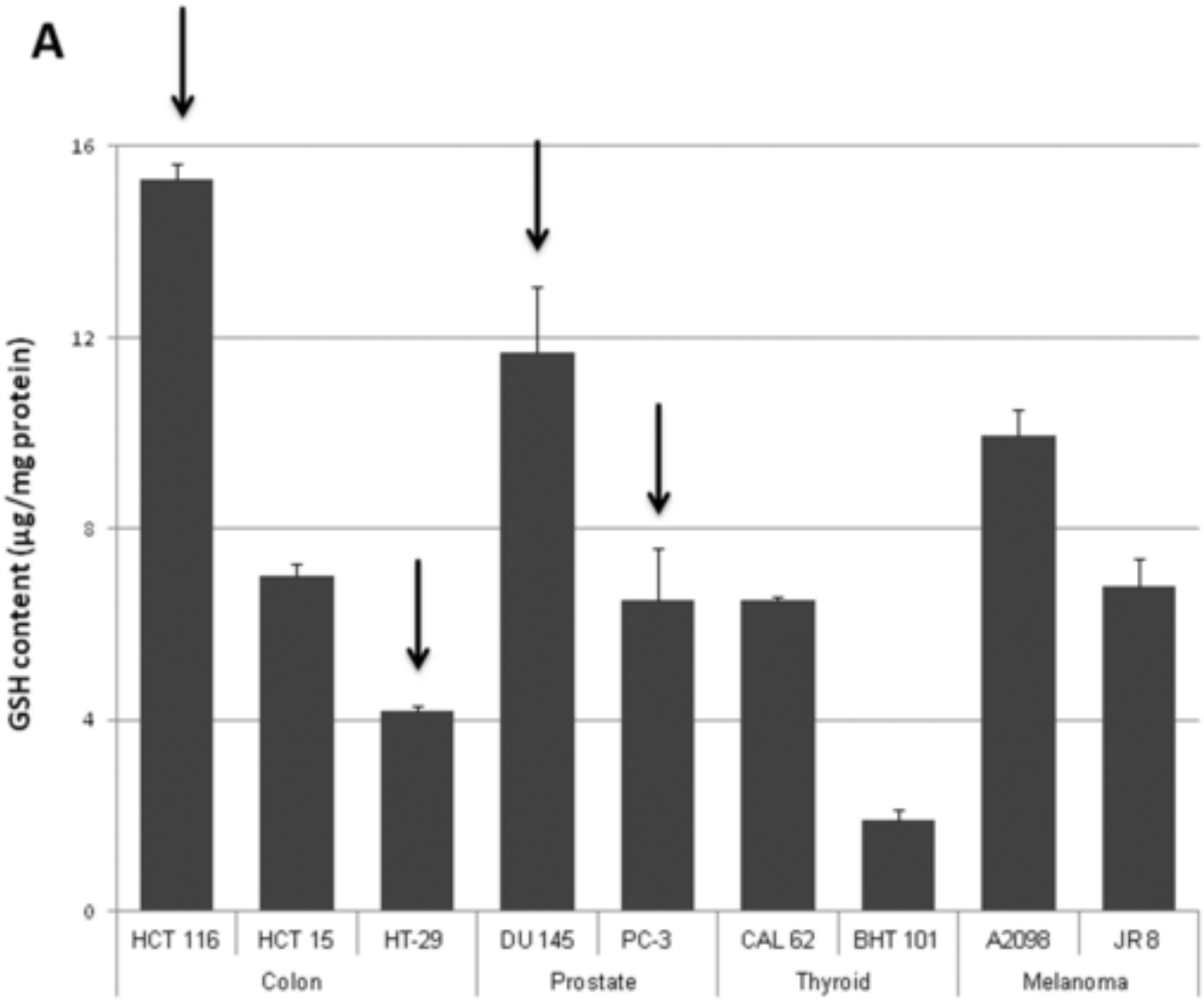

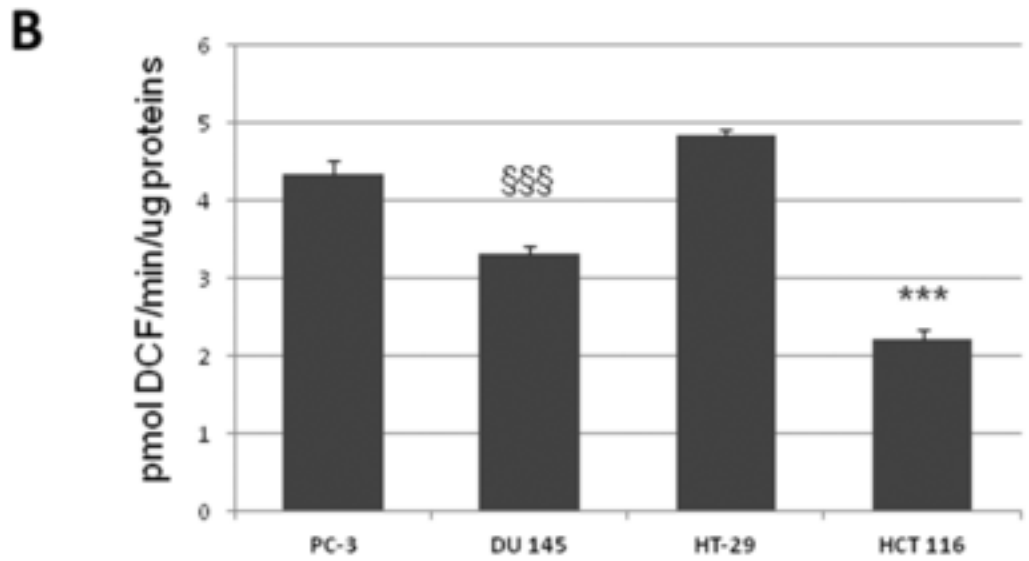

Figure 2

Click here to download high resolution image

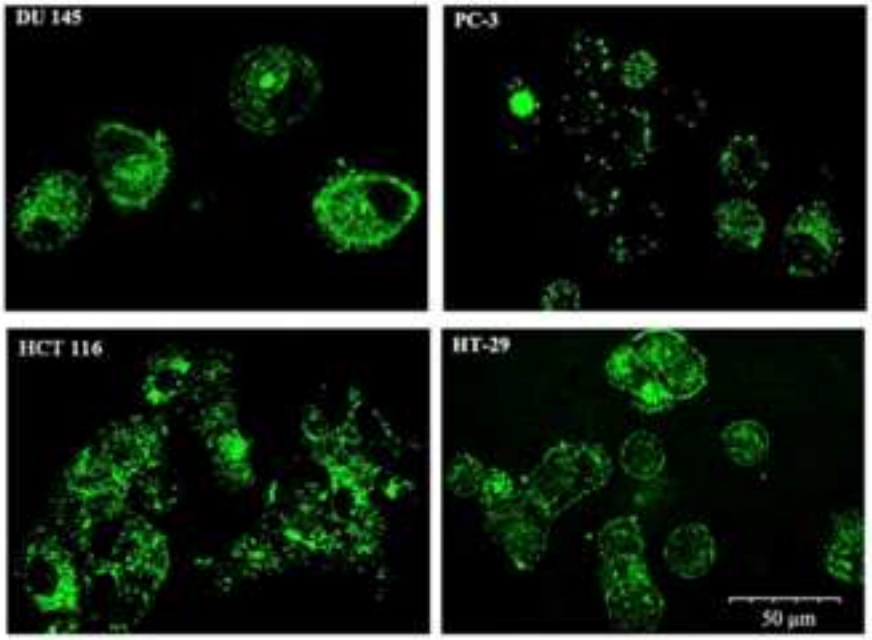

Figure 3

Click here to download high resolution image

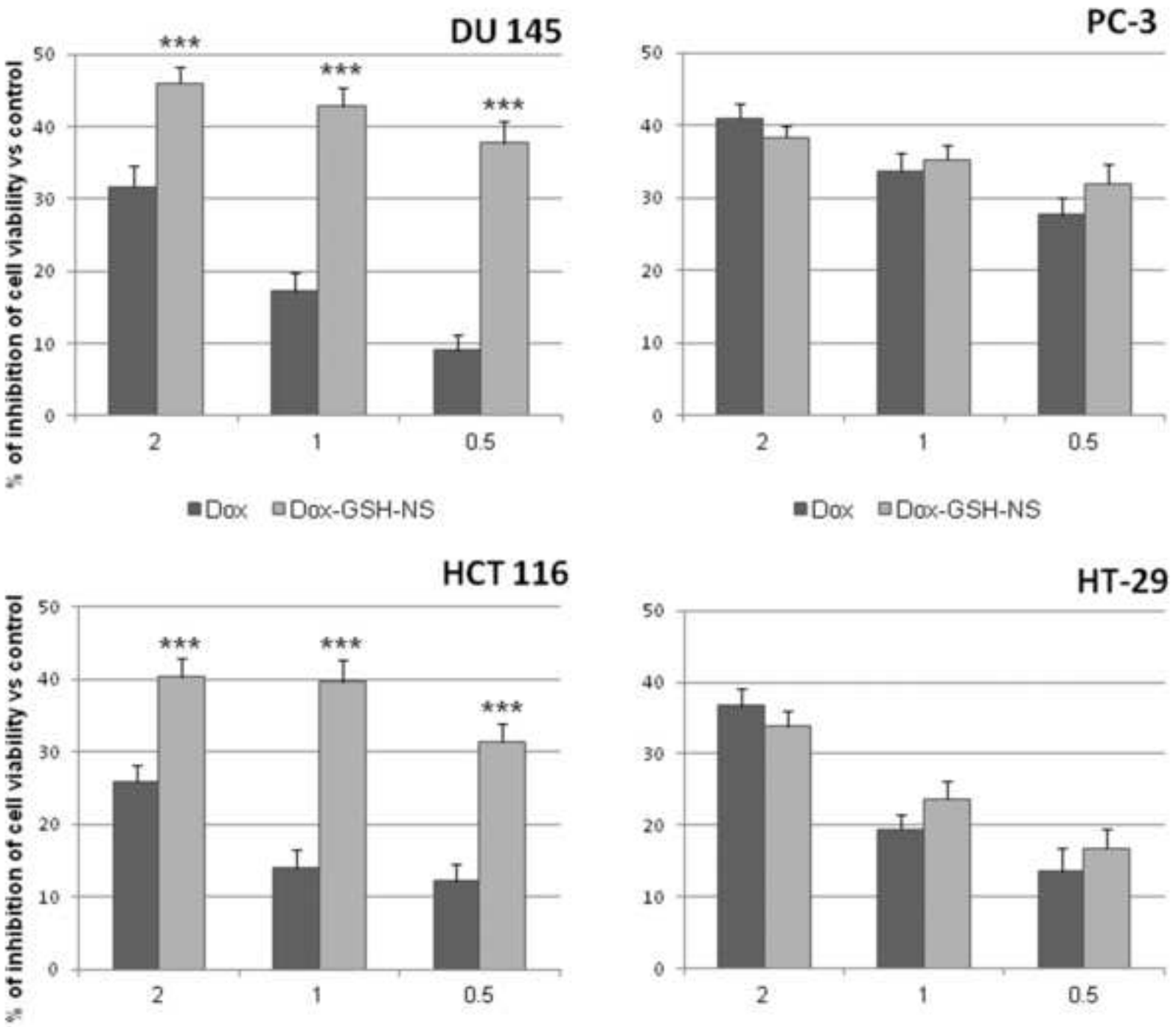

Figure 4

Click here to download high resolution image

A

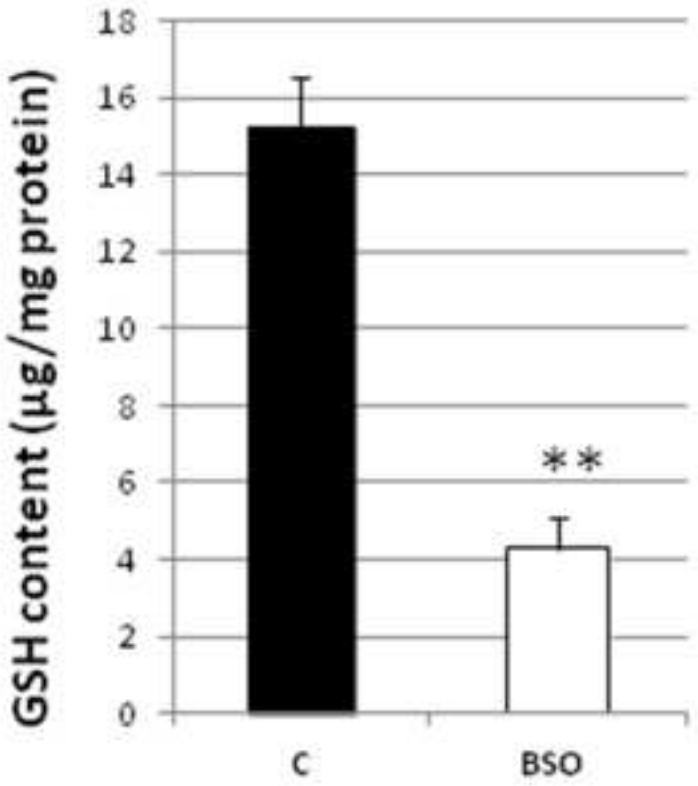

B

Table 1

	w/o BSO		with BSO	
	Dox	Dox-GSH-NS	Dox	Dox-GSH-NS
2 µg/ml	32.3 ± 1.5	47.6 ± 1.8***	38.7 ±3.4	42.4 ± 2.3
1 µg/ml	19.7 ± 0.3	39.7 ± 2.3***	25.6 ± 3.2	32.2 ± 2.9
0.5 µg/ml	15.4 ± 2.4	35.5 ± 2.3***	27.9 ± 6.5	32.8 ± 6.7

Figure 5

Click here to download high resolution image

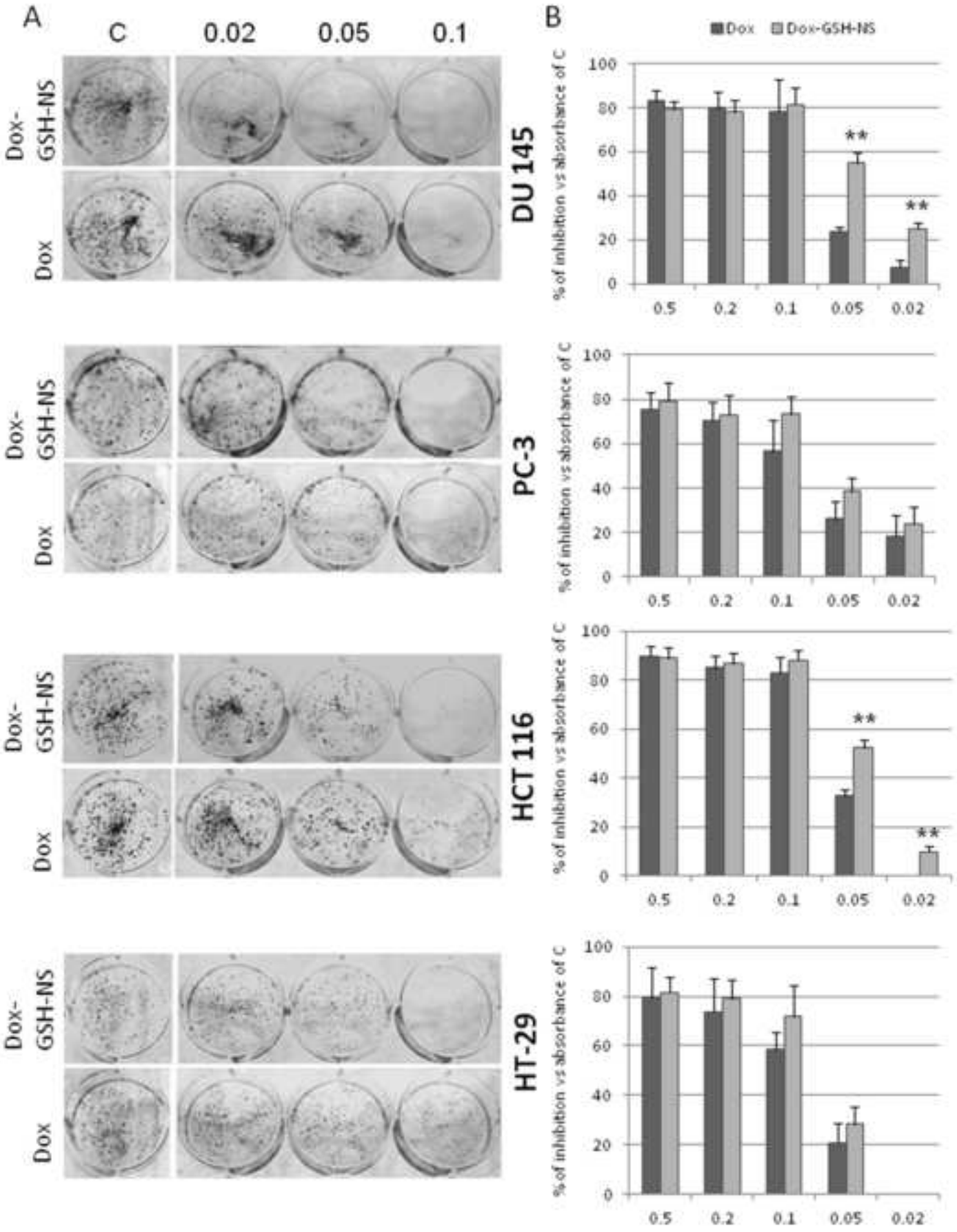

Figure 6

Click here to download high resolution image

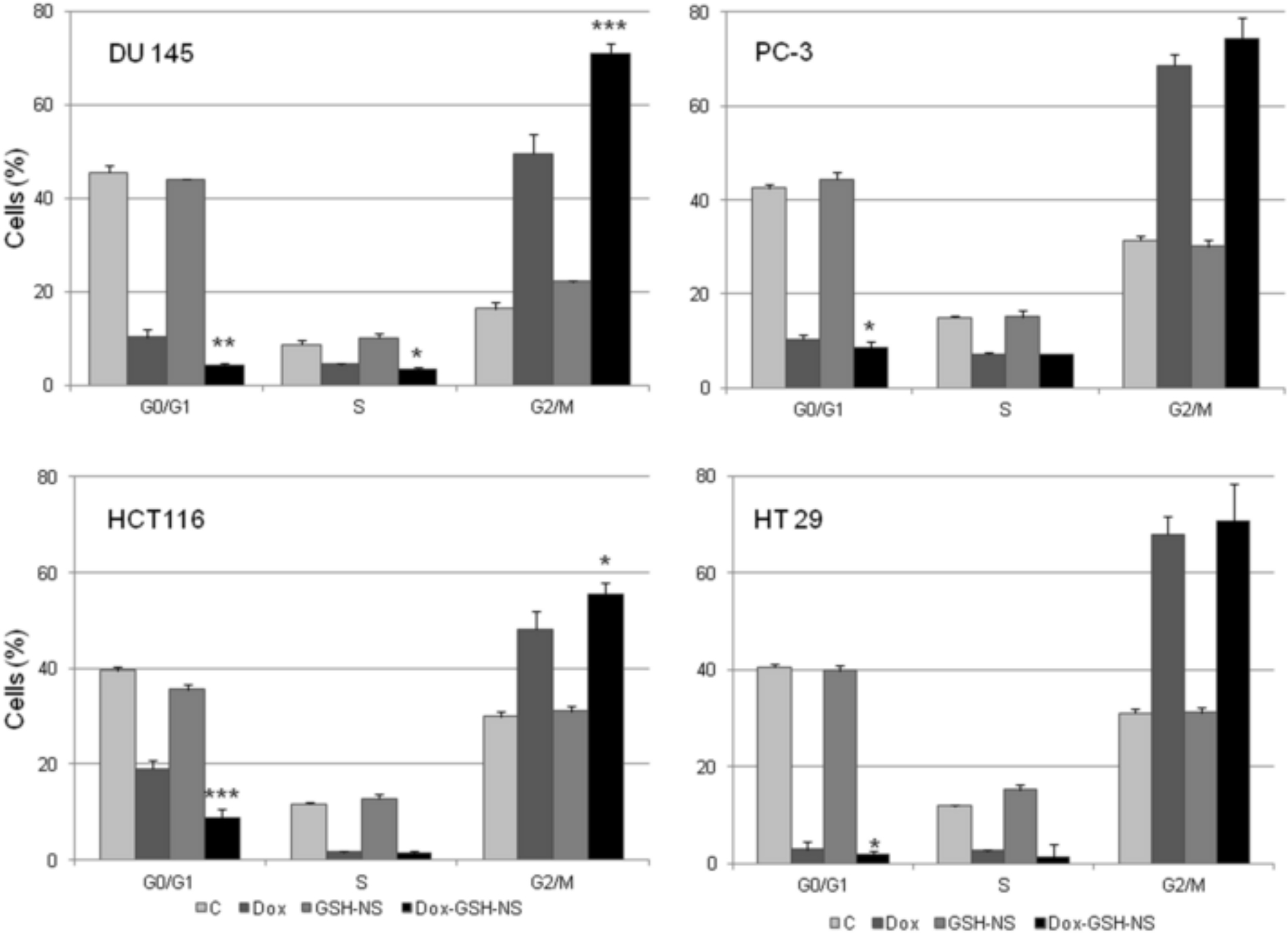

Figure 7

Click here to download high resolution image

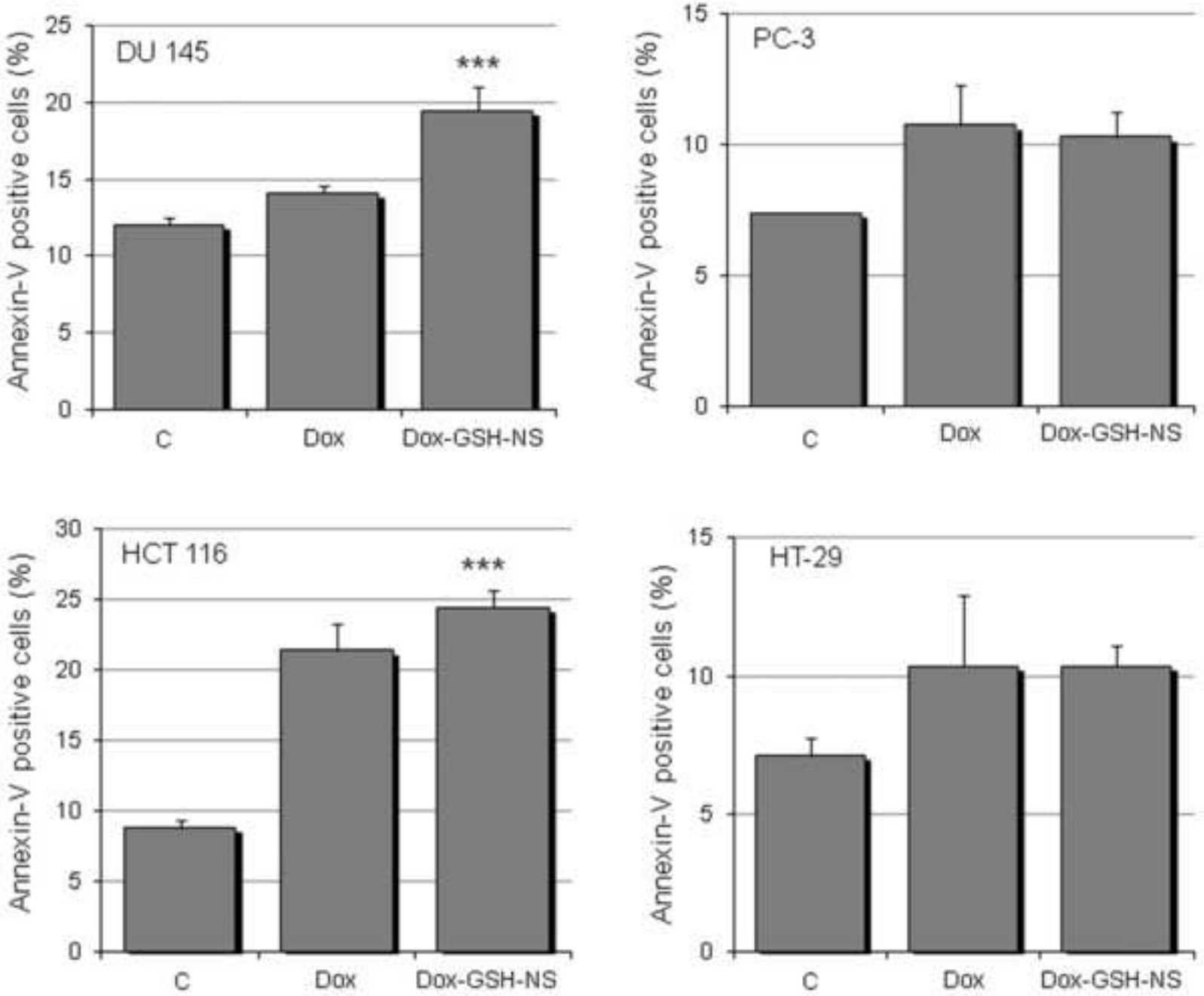

Figure 8

Click here to download high resolution image

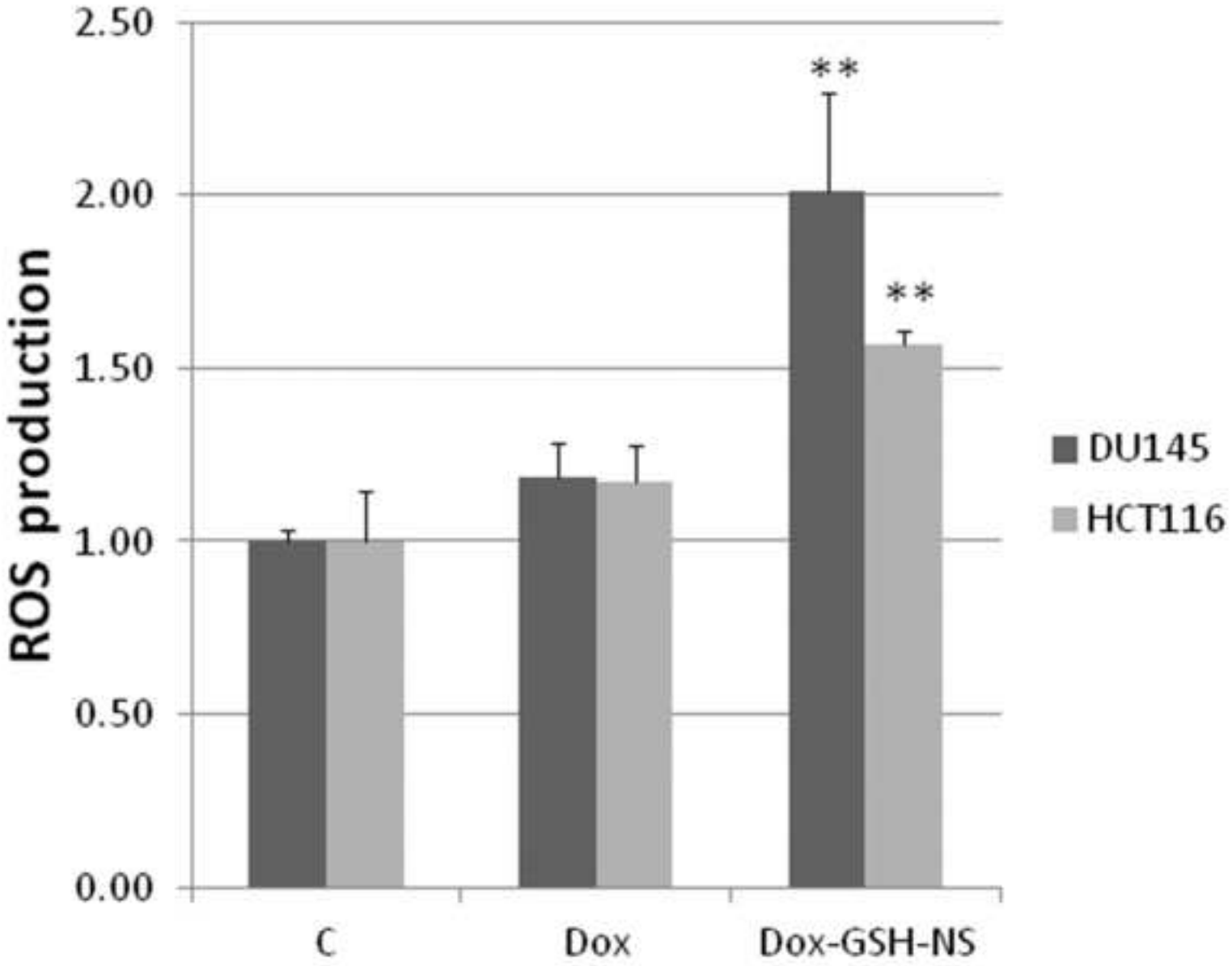

Figure 9

Click here to download high resolution image

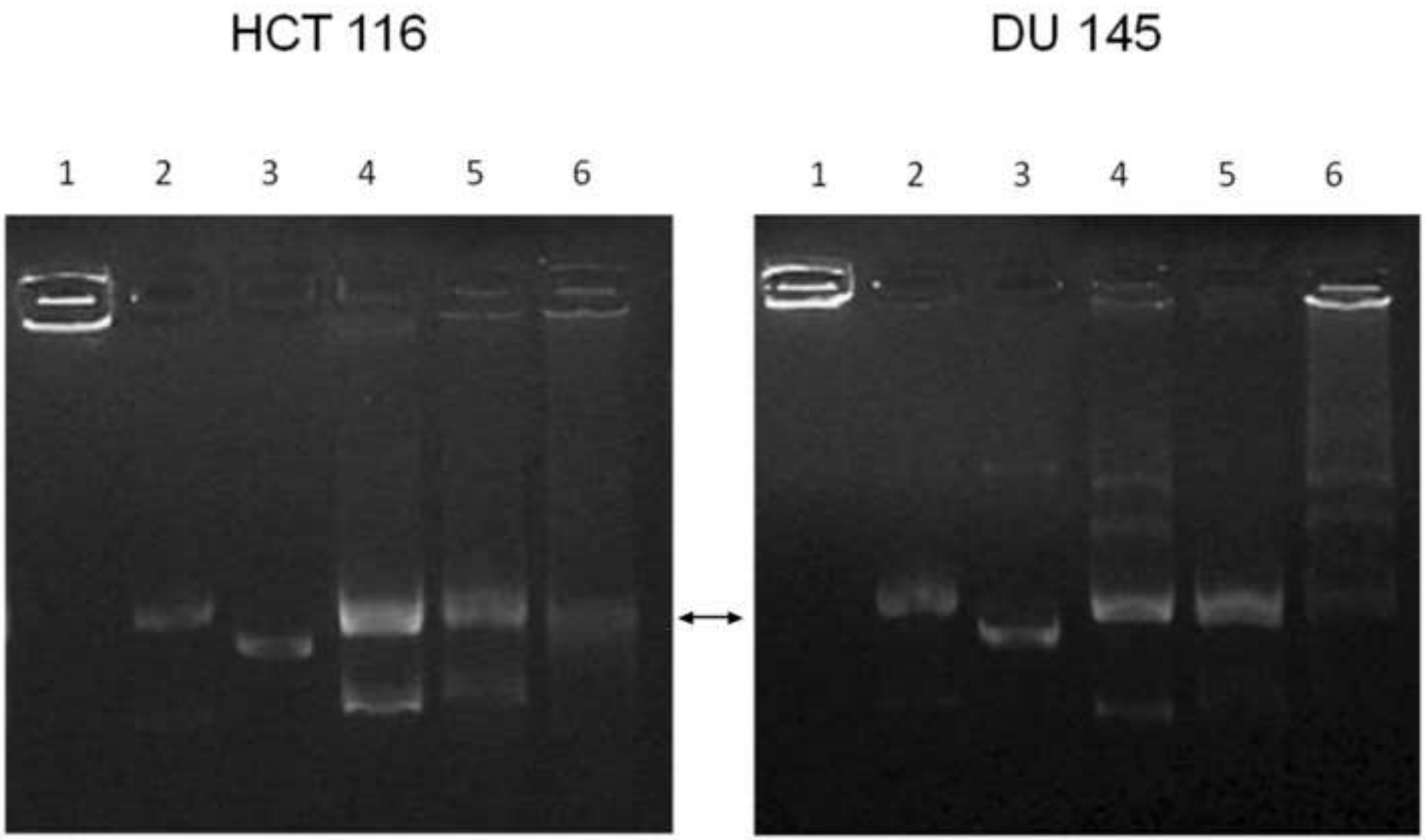

Figure 10

Click here to download high resolution image

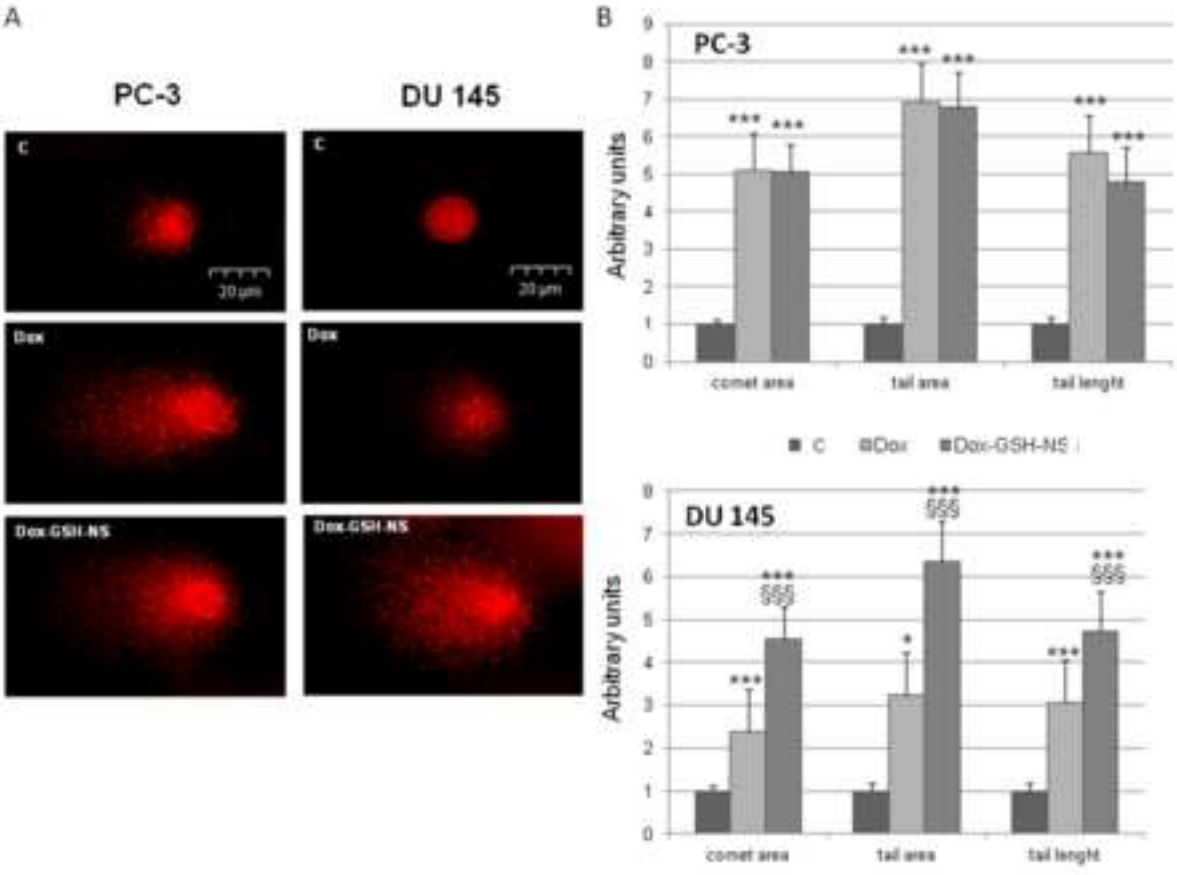

Figure 11

Click here to download high resolution image

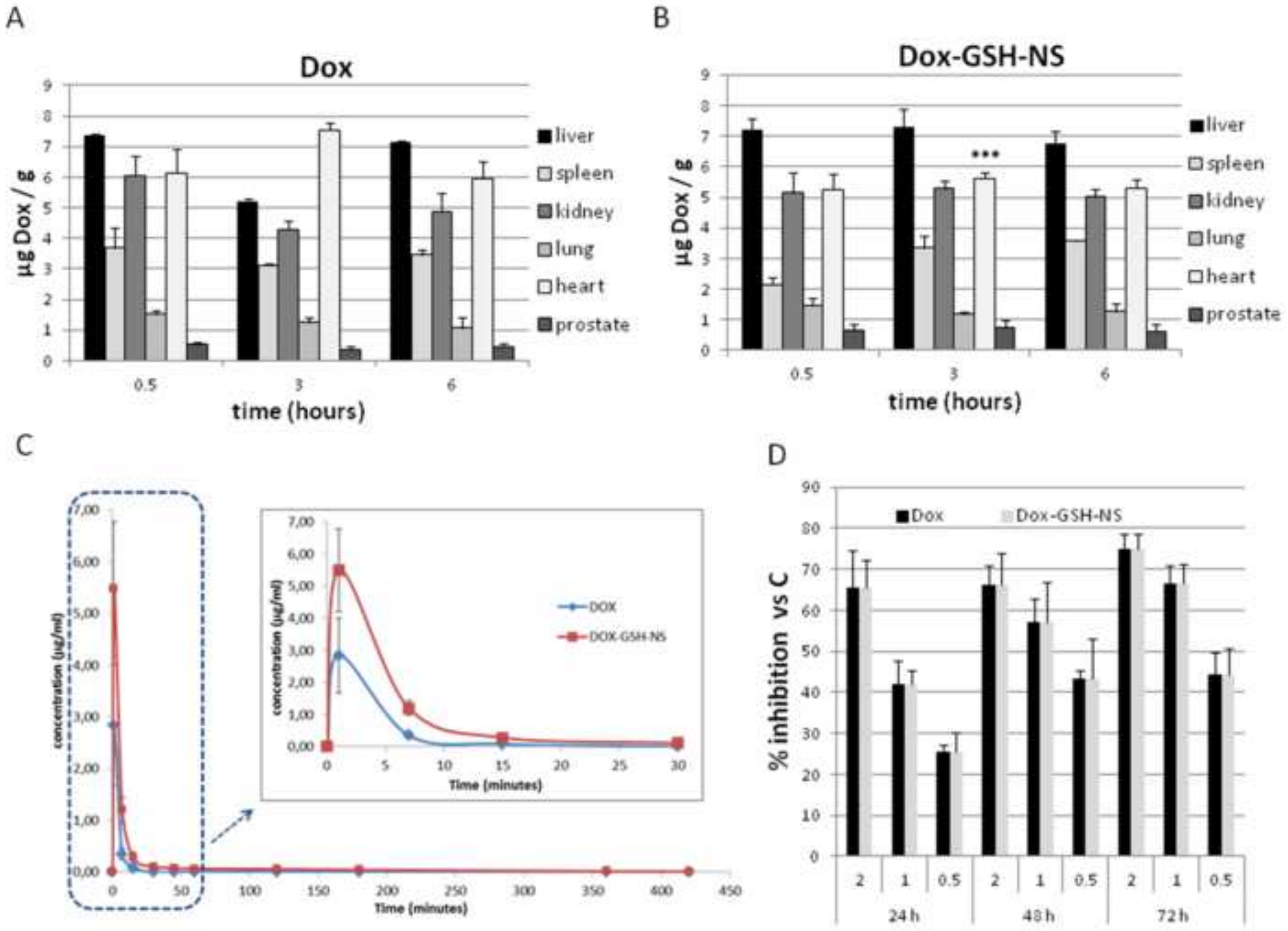

Figure 12

Click here to download high resolution image

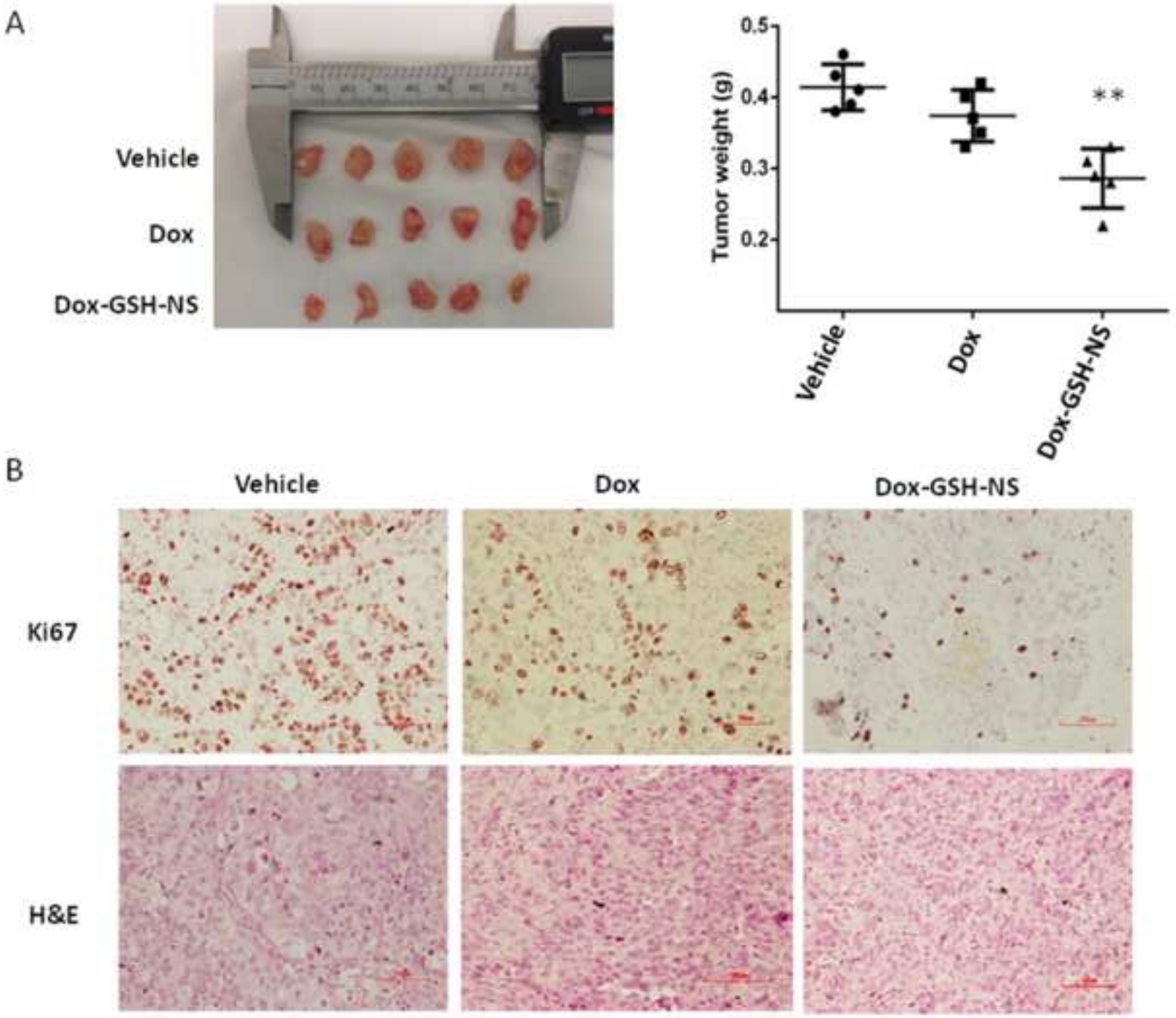

Figure Supplementary S_1

Click here to download high resolution image

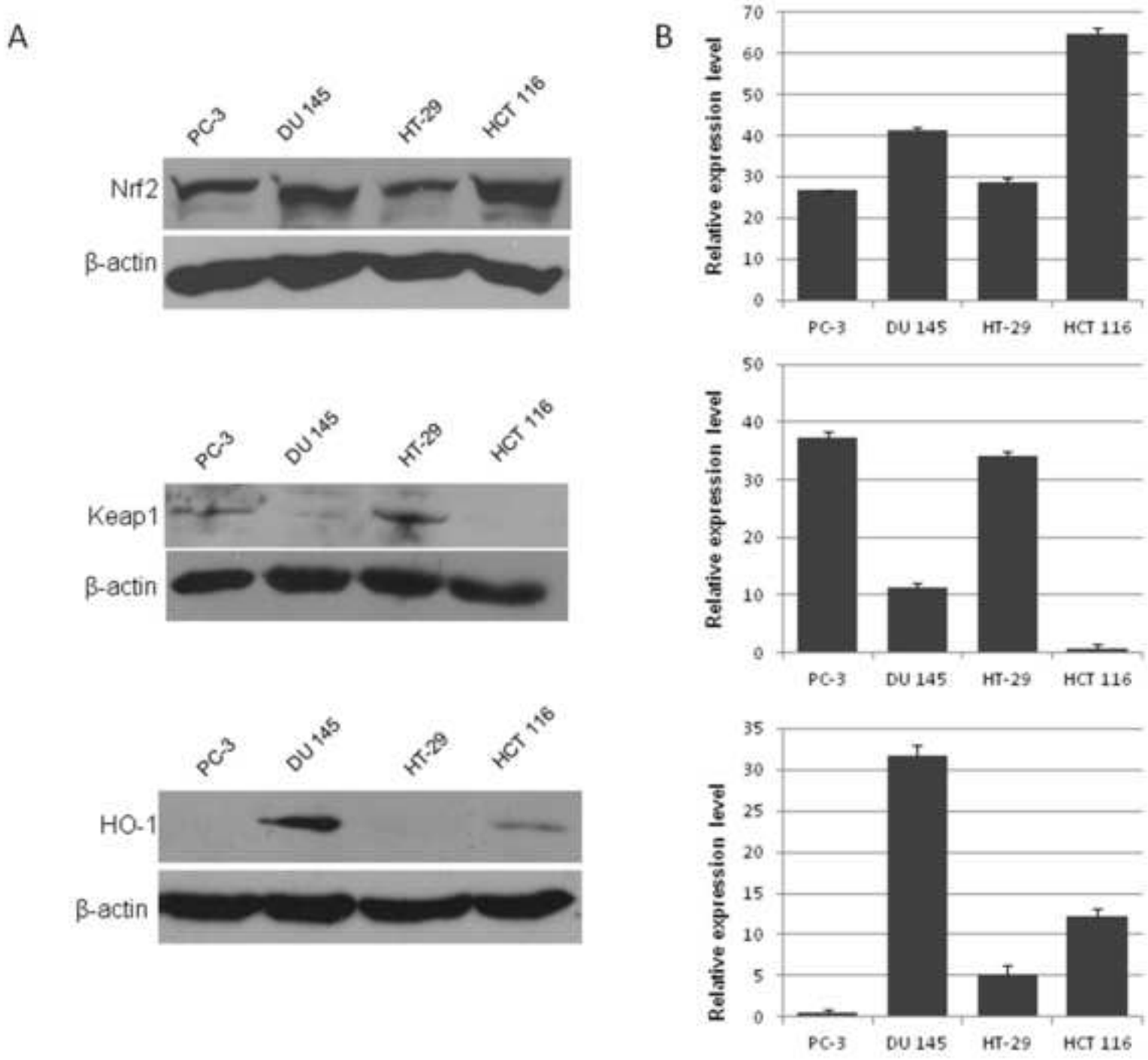

Figure Supplementary S_2

Click here to download high resolution image